Atmospheric
Chemistry
and Physics
Discussions

Open Access

EGU

1   **Formation, radiative forcing, and climatic effects of severe regional haze**

2   Yun Lin[1,2*], Yuan Wang[3*], Bowen Pan[1,4], Jiaxi Hu[1,5], Song Guo[6], Misti Levy Zamora[1,7],

3   Pengfei Tian[1,8], Qiong Su[9], Yuemeng Ji[1,10], Jiayun Zhao[11], Mario Gomez-Hernandez[11], Min

4   Hu[6], Renyi Zhang[1,11*]

5   [1]Department of Atmospheric Sciences, Texas A&M University, College Station, TX 77843,
6   USA
7   [2]Joint Institute for Regional Earth System Science and Engineering (JIFRESSE), University
8   of California at Los Angeles, Los Angeles, CA 90064
9   [3]Division of Geological and Planetary Sciences, California Institute of Technology,
10   Pasadena, CA 91125, USA
11   [4]Department of Atmospheric Science, Colorado State University, Fort Collins, CO, 80521,
12   USA
13   [5]Cooperative Institute for Mesoscale Meteorological Studies, NOAA/OAR National Severe
14   Storms Laboratory, Norman, OK, USA
15   [6]State Key Joint Laboratory of Environmental Simulation and Pollution Control, College of
16   Environmental Sciences and Engineering, Peking University, Beijing, 10087, P.R. China
17   [7]Department of Environmental Health and Engineering, Johns Hopkins Bloomberg School of
18   Public Health, 615 N. Wolfe St., Baltimore, MD 21205, USA
19   [8]Key Laboratory for Semi-Arid Climate Change of the Ministry of Education, College of
20   Atmospheric Sciences, Lanzhou University, Lanzhou 730000, P. R. China
21   [9]Water Management & Hydrological Science, Texas A&M University, College Station, TX
22   77843, USA
23   [10]Guangzhou Key Laboratory of Environmental Catalysis and Pollution Control, School of
24   Environmental Science and Engineering, Institute of Environmental Health and Pollution
25   Control, Guangdong University of Technology, Guangzhou 510006, China
26   [11]Department of Chemistry, Texas A&M University, College Station, TX 77843, USA
27
28   *Correspondence: yunlin@ucla.edu; Yuan.Wang@caltech.edu; renyi-zhang@tamu.edu

29

30 **Abstract.** Severe regional haze events, which are characterized by exceedingly high levels of

31 fine particulate matter (PM), occur frequently in many developing countries (such as China

32 and India), with profound implications for human health, weather, and climate. The occurrence

33 of the haze extremes involves a complex interplay between primary emissions, secondary

34 formation, and conducive meteorological conditions, and the relative contributions of the

35 various processes remains unclear. Here we investigated severe regional haze episodes in 2013

36 over the Northern China Plain (NCP), by evaluating the PM production and the interactions

37 between elevated PM and the planetary boundary layer (PBL). Analysis of the ground-based

38 measurements and satellite observations of PM properties shows nearly synchronized temporal

39 PM variations among the three megacities (Beijing, Baoding, and Shijiazhuang) in this region

40 and a coincidence of the aerosol optical depth (AOD) hotspots with the three megacities during

41 the polluted period. During the clean-to-hazy transition, the measured oxygenated organic

42 aerosol concentration ([OOA]) well correlates with the odd-oxygen concentration ($[O_x] = [O_3]$

43 $+ [NO_2]$), and the mean $[OOA]/[O_x]$ ratio in Beijing is much larger than those in other

44 megacities (such as Mexico City and Houston), indicating highly efficient photochemical

45 activity. Simulations using the Weather Research and Forecasting (WRF) model coupled with

46 an explicit aerosol radiative module reveal that strong aerosol-PBL interaction during the

47 polluted period results in a suppressed and stabilized PBL and elevated humidity, triggering a

48 positive feedback to amplify the haze severity at the ground level. Model sensitivity study

49 illustrates the importance of black carbon (BC) in the haze-PBL interaction and the aerosol

50 regional climatic effect, contributing to more than 30% of the PBL collapse and about half of

51 the positive radiative forcing on the top of the atmosphere. Overall, severe regional haze

52 exhibits strong negative radiative forcing (cooling) of -63 to -88 W m^{-2} at the surface and strong

53 positive radiative forcing (warming) of 57 to 82 W m^{-2} in the atmosphere, with a slightly

54 negative net radiative forcing of about -6 W m^{-2} on the top of the atmosphere. Our work

55   establishes a synthetic view for the dominant regional features during severe haze events,

56   unraveling rapid *in-situ* PM production and inefficient transport, both of which are amplified

57   by atmospheric stagnation. On the other hand, regional transport sufficiently disperses gaseous

58   aerosol precursors (e.g., sulfur dioxide, nitrogen oxides, volatile organic compounds, and

59   ammonia) during the clean period, which subsequently result in rapid *in-situ* PM production

60   via photochemistry during the transition period and via multiphase chemistry during the

61   polluted period. Our findings highlight the co-benefits for reduction in BC emissions, which

62   not only improve local and regional air quality by minimizing air stagnation but also mitigate

63   the global warming by alleviating the positive direct radiative forcing.

64

65

66

1. Introduction

67

68   Rapid economic growth and urbanization have caused frequent severe regional haze

69 events associated with heavy pollution of particulate matter (PM) in many developing countries,

70 including China and India (Bouarar et al., 2017; Molina, 2021). The severe haze events induce

71 great degradation in visibility and air quality, with profound societal implications (An et al.,

72 2019). For example, exposure to elevated levels of fine PM leads to adverse health effects,

73 ranging from aggravated allergies to the development of chronic diseases, to premature death

74 (Pope and Dockery, 2015; Wu et al., 2019; Rychlik et al., 2019; Johnson et al., 2021; Zhang et

75 al., 2021). Also, elevated levels of fine aerosols result in pronounced modifications to clouds,

76 precipitation, and lightning, impacting regional/global weather and climate (Zhang et al., 2007;

77 Yuan et al., 2008; Qian et al., 2009; Wang et al., 2011; Wang et al., 2014; Wu et al., 2016).

78 Specifically, by absorbing/scattering solar radiation, aerosols impact the atmospheric stability

79 and the energy budget of Earth, via the aerosol-radiation interaction (ARI). By serving as cloud

80 condensation nuclei (CCN) and ice nucleating particles (INPs), aerosols influence the macro-

81 and microphysical properties of clouds, via the aerosol–cloud interaction (ACI). Currently, the

82 radiative forcing associated with ARI and ACI represents the largest uncertainty in the

83 projection of future climate by anthropogenic activities (IPCC, 2013).

84   PM is either emitted directly into the atmosphere (primary) or produced in air via gas-

85 to-particle conversion (secondary) (Zhang et al., 2015a). In addition, primary and secondary

86 PM undergo chemical and physical transformations and are subjected to cloud processing and

87 removal from air (Zhang et al., 2015a). Direct emissions of primary gases and PM and highly

88 efficient secondary PM formation represent the primary processes leading to severe haze (Guo

89 et al., 2014; Sun et al., 2014; Wang et al., 2016a; Peng et al., 2021). In addition, conducive

90 weather conditions for pollutant accumulation, such as regional control by high-pressure,

91 suppressed local circulations, and weakened large-scale circulation, correspond to the external

Atmospheric
Chemistry
and Physics
Discussions

Open Access

EGU

92   causes for severe haze formation (Liu et al., 2013; Wang et al., 2014d; Cai et al., 2017; Li et

93   al., 2019).

94   The key constituents of fine PM include secondary inorganic (including sulfate, nitrate,

95   and ammonium) aerosol (SIA) and secondary organic aerosol (SOA), with the corresponding

96   gaseous precursors of sulfur dioxide (SO_2), nitrogen oxides ($NO_x = NO + NO_2$), ammonia

97   (NH_3), and volatile organic compounds (VOCs). The photochemistry represents one of the

98   mechanisms leading to SIA and SOA accumulation during the early stage of haze evolution

99   (Guo et al., 2014; Zhang et al., 2015a;   Wang et al., 2016; Zhang et al., 2020). Field

100   measurements have shown that remarkably nucleation and growth of nanoparticles are

101   primarily driven by photochemical activity, which is characterized by elevated ozone levels

102   and efficient photolysis rate coefficients under clean daytime conditions (Zhang et al., 2015b;

103   Guo et al., 2020). During haze evolution, the photochemical activity is typically reduced, as

104   evident by low levels of ozone and reduced photolysis rates (Peng et al., 2021). On the other

105   hand, there are increasing air stagnation and relative humidity (RH), when explosive secondary

106   aerosol formation occurs (Peng et al., 2021). The latter has been attributed the occurrence of

107   multiphase chemistry, which largely drives the formation of SIA and SOA during the polluted

108   period (Peng et al., 2021). Currently, the relative contributions of primary emissions, secondary

109   production, and regional transport to severe haze formation remain uncertain (Li et al., 2015;

110   Zhang et al., 2015b; Peng et al., 2021). Moreover, the efficiency of photochemical PM

111   production during regional haze events in NCP and its distinction among various megacities

112   worldwide remain to be quantified (Molina, 2021).

113   While the importance of regional haze on climate has been recognized (Ramanathan et

114   al., 2007; Wang et al., 2009; Wang et al., 2015a), there still lacks quantification for the aerosol

115   radiative forcing and the climatic effects for severe regional haze events. Estimation of the

116   aerosol radiative forcing during severe haze events exhibits a large variation (Li et al., 2007;

117 Xia et al., 2007; Wang et al., 2009; Che et al., 2014). In addition, the interactions between

118 aerosols and planetary boundary layer (PBL) via the aerosol radiative effects likely increase

119 the haze severity (Wang et al., 2015a; Wang et al., 2016b; Zhang et al., 2018). Meteorological

120 conditions within the PBL, including the atmospheric stability and RH, are altered by the

121 aerosol-PBL interaction to induce a positive feedback to PM accumulation near the ground

122 level (Tang et al., 2016a; Tie et al., 2017; Wu et al., 2020). However, the aerosol-PBL

123 interactions and their feedbacks to atmospheric thermodynamics and dynamics under

124 extremely hazy conditions remain to be quantified (Li et al., 2017).

125 Previous studies have documented the role of black carbon (BC) in the aerosol-PBL

126 interactions and the aerosol regional climate effects (Menon et al., 2002; Bond et al., 2013;

127 Wang et al., 2013; Ding et al., 2016). In addition, the BC aging process markedly enhances BC

128 absorption by modifying the particle physiochemical and optical properties (Zhang et al., 2008;

129 Khalizov et al., 2013; He et al., 2015; Guo et al., 2016; Peng et al., 2016; Peng et al., 2017).

130 For example, an experimental/field study showed that the mass absorption cross section (MAC)

131 of BC is enhanced by 2.4 times in a short time because of BC aging under polluted urban

132 conditions (Peng et al., 2016), reconciling previous variable results on the coating-enhanced

133 absorption for BC (Gustafsson and Ramanathan, 2016). Apparently, the enhancement of the

134 BC absorption causes additional aerosol radiative forcing (Peng et al., 2016) and suppression

135 on PBL development (Wang et al., 2017). Currently, limited modeling studies have assessed

136 the radiative effect of BC aging associated with severe regional haze (Wang et al., 2013; He et

137 al., 2015; Gustafsson and Ramanathan, 2016).

138 To better understand the formation and evolution of severe regional haze as well as

139 their regional and climate effects, we investigated severe haze episodes occurring in 2013 over

140 the Northern China Plain (NCP). The NCP region, which encompasses the megacities of

141 Beijing and Tianjin, and some portion of the provinces of Heibei, Shandong, and Henan,

Atmospheric
Chemistry
and Physics
Discussions

Open Access

EGU

142 represents the most polluted area in China (An et al., 2019). Satellite observations and field

143 measurements of PM properties were evaluated, and numerical simulations were performed to

144 elucidate the interactions between severe haze and PBL using Weather Research and Forecast

145 (WRF) model coupled with an explicit aerosol radiative module (Fan et al., 2008; Wang et al.,

146 2014c). By conducting model sensitivity simulations, we elucidated the impacts of BC aging

147 on the haze-PBL interactions and its contribution to the net aerosol radiative forcing during

148 severe haze periods.

149 **2. Methodology**

150   The NCP represents a key economic zone in China, as reflected by its gross domestic

151 product (GDP), energy consumption, and vehicular fleets (An et al., 2019). The region has

152 undergone fast industrialization and urbanization over the past four decades. For example, NCP

153 is one of the most densely populated regions in the world and contributes to over 1/10 of the

154 GDP in China. The consumption of coal and crude oil in NCP was 363 and 72 million tons,

155 respectively, to 1,348 million tons in 1998 and increased to 140 million tons of standard coal

156 equivalent in 2010, respectively. In particular, anthropogenic activities result in industrial,

157 traffic, residential, and agricultural emissions, representing the major sources for PM

158 precursors, including SO_2, NO_x, VOCs, and NH_3 (An et al., 2019; Peng et al., 2021).

159 Surrounded by the Taihang Mountains to the west and Yanshan Mountains to the north,

160 respectively, the NCP region is prone to develop air stagnation under conducive meteorological

161 conditions, inhibiting vertical and horizontal dispersion of air pollutants (An et al., 2019; Peng

162 et al., 2021).

163 **2.1. The Data Sources**

164   The satellite-retrieved aerosol optical depth (AOD) was derived by combining the

165 Moderate Resolution Imaging Spectroradiometer (MODIS) measurements of Aqua and Terra

166 using the equal-weighted mean method to increase the spatial coverage (Levy et al., 2009). The

167   MODIS data are accessible at http://giovanni.gsfc.nasa.gov/aerostat/. The Terra visible images

168   were obtained at https://worldview.earthdata.nasa.gov/. The hourly PBL height used was based

169   on the Modern-Era Retrospective analysis for Research and Applications, Version 2 (MERRA2)

170   reanalysis data. The severe haze days were selected with daily $PM_{2.5}$ (particular matter with

171   aerodynamic diameter less than 2.5 micron) concentration greater than 200 μg m^{-3}, and the

172   typical clean days were limited to the days with daily $PM_{2.5}$ concentration smaller than 30 μg

173   m^{-3}. The PBL height and the $PM_{2.5}$ surface concentration at 14:00 Beijing time (BJT) each day

174   in 2013 were used for the correlation analysis. All raining days were filtered out when

175   analyzing the correlation between the PBL height and the $PM_{2.5}$ concentration. The surface

176   solar radiation (SSR) data were based on the satellite retrievals (Tang et al., 2016b), which are

177   accessible at http://www.tpedatabase.cn.

178   Ground-based measurements of fine particulate matter or $PM_{2.5}$ employed in our

179   analysis covered the period from 25 September to 14 November 2013. The hourly $PM_{2.5}$

180   concentrations in Beijing (BJ) were obtained from the Embassy of United States in Beijing

181   (http://www.stateair.net/web/historical/1/1.html). The $PM_{2.5}$ mass concentrations in Baoding

182   (BD) and Shijiazhuang (SJZ) were obtained from https://air.cnemc.cn:18007/. Measurements

183   of PM properties in Beijing were taken from that previously reported by Guo et al. (2014),

184   which provided $PM_{2.5}$ concentration, aerosol chemical composition, and gaseous data for

185   correlation analysis and constrains for modeling studies. The observation-based analysis and

186   the modeling study focused on two severe haze episodes, i.e., 25 September – 30 September

187   (episode 1 or EP1) and 2 October – 6 October (episode 2 or EP2), 2013 in NCP.

188   **2.2. Model experiments**

189   **2.2.1. Simulations on the haze-PBL interactions**

190   The aerosol-PBL interactions during the severe haze events and the associated regional

191   climate effects were examined by conducting WRF modeling sensitivity studies. An aerosol

Atmospheric
Chemistry
and Physics
Discussions

Open Access

EGU

192   radiative module was implemented by Fan et al. (2008) to the Goddard Shortwave Radiation

193   Scheme to online compute the wavelength-dependent aerosol optical properties, including the

194   AOD, the asymmetry factor and the single scattering albedo (SSAs). Aerosol particles with the

195   core-shell configuration in the aerosol radiative module were assumed to consist of BC (core)

196   and ammonia sulfate (shell). The hygroscopic growth of aerosol particles was taken into

197   account, following Mallet et al. (2004). A two-moment bulk microphysical scheme developed

198   by Li et al. (2008) was employed, which has been widely used to investigate the aerosol-cloud

199   interactions under various cloud systems (Wang et al., 2014b; Wang et al., 2014a; Lin et al.,

200   2016). A 100×100 grids domain with a horizontal grid spacing of 2 km and 50 vertical levels

201   with stretched grid spacings was set up to cover the entire urban region of Beijing. The initial

202   and boundary meteorological conditions were generated from six-hourly NCEP FNL (Final)

203   Operational Global Analysis (1°×1°). No convective parametrization was applied for the

204   simulations.

205   We performed simulations on the two haze episodes (EP1 and EP2). The two days prior

206   to the two haze episodes (25 September and 2 October, 2013) are denoted as the clean periods,

207   while the most polluted days during the two episodes, i.e., 28 September and 5 October are

208   denoted as the polluted periods. The aerosol number size distributions for initial and boundary

209   conditions of all simulation were based on the measurements during the 2013 field campaign

210   at Beijing (Fig. S1). The aerosol measurements on 25 September and 2 October 2013 were

211   taken as the input for the clean cases and 28 September and 5 October 2013 for the polluted

212   cases. The aerosol surface number and mass concentration for modeling initialization were set

213   as $3.5×10^4$ cm^{-3} ($3.6×10^4$ cm^{-3}) and 10 µg m^{-3} (11 µg m^{-3}) for the clean case of EP1 (EP2) and

214   $1.7×10^4$ cm^{-3} ($1.8×10^4$ cm^{-3}) and 280 µg m^{-3} (310 µg m^{-3}) for the polluted case of EP1 (EP2),

215   respectively, consistent with the field measurements. Also, based on the measurements, the BC

216   percentage in total aerosol mass was set as 10.0% and 6.0% for the clean and polluted cases,

217 respectively. The two polluted days for simulations were cloud-free days, therefore the aerosol

218 indirect effects were ruled out.

219 To assess the role of BC in the aerosol suppression effect on the PBL development and

220 the aerosol radiative forcing during haze evolution, we performed a set of sensitivity

221 simulations under the polluted condition by excluding the BC effects (referred as non-BC case),

222 in which the BC radiative effect was turned off by assigning a zero value to the real and

223 imaginary parts of BC refractive index, i.e., the SSA in non-BC case was equal to unity. To

224 quantify the BC aging effects, additional simulations were carried out for fresh BC (denoted

225 by fresh-BC), in which the BC core was not imbedded in the non-BC shell and the optical

226 parameters for the BC and non-BC components were calculated separately by the Mie theory.

227 In the fresh-BC case, the lensing effect due to the coating during the aging process was

228 excluded, but the restructuring effect induced by aging was considered partially since the BC

229 core was assumed to be spherical and in the compact shape. Alternatively, a case for aged BC

230 (denoted by aged-BC) was treated by considering the full aerosol components (with both BC

231 and non-BC components) and the core-shell configuration. A summary of the simulation cases

232 is listed in Table 1.

233 One deficiency to predict the absorbed AOD and the directive radiation forcing of BC

234 in atmospheric models is relevant to the underestimation in coating-enhancement of BC

235 absorption (Bond et al., 2013). To assess the potential bias on the radiative effects of aged BC,

236 additional simulations on the polluted conditions were conducted by constraining the

237 enhancement of mass absorption cross section of BC (E_{MAC-BC}) according to the experimental

238 value, i.e., 2.4, derived from a chamber study in Beijing (Peng et al., 2016). Though the E_{MAC-BC}

239 of 2.3 derived from the aged-BC case is slightly lower than that reported by Peng et al.

240 (2016), comparison between the two simulations indicates little difference in the

241 thermodynamic/dynamic conditions and the radiative budget.

Atmospheric
Chemistry
and Physics
Discussions

2.2.2. Empirical estimation of the moisture effect on haze-PBL interactions

In addition to the numerical model simulations, we employed an empirical equation derived by Nozaki (1973) and modified by Tie et al. (2017) to examine the RH sensitivity in the boundary layer to the PBL height based on observed meteorological conditions:

$$H = \frac{121}{6}(6 - P)(T - T_d) + \frac{0.169P(U_Z + 0.257)}{12f \ln Z/z_0} \qquad (1)$$

where H, T, T_d, and U_z represent the PBL height (m), surface air temperature (K), surface dew point (K), and mean wind speed (m s⁻¹) at height of Z (Z=10 m), respectively. f and z_0 are the Coriolis parameter (s⁻¹) and surface roughness length (0.5 m in this study), respectively. P is the Pasquill stability level, classified as six categories from very unstable (A), moderately unstable (B), slightly unstable (C), neutral (D), slightly stable (E) to moderately stable (F) (Pasquill, 1961). To relate RH with the PBL height, we adopted a modified Nozaki's equation using (100- RH)/5 to replace (T-T_d) according to Wallace and Hobbs (2005) and Tie et al. (2017). The measured wind speeds were used in the calculations. For the severe haze events, the atmosphere was stable, and the Pasquill stability levels were set as 4~5. The input of the PBL height for the aged-BC cases were based on ceilometer measurements, and we increased the PBL height by about 1000 m as the input for the clean cases, which was estimated based on MERRA2 reanalysis data due to the lack of relevant measurements.

3. Results and Discussion

3.1. Regional characteristics of severe haze episodes

Measurements of the PM$_{2.5}$ mass concentrations from 25 September to 14 November 2013 reveal that severe haze occurs frequently over the NCP, reflected by a periodic cycle of 4-7 days with highly elevated PM pollution (Fig. 1a-c). Each severe haze episode consists of a clean period, a transition period from clean to hazy conditions, and a polluted period with very high PM levels. For the three megacities across the NCP, i.e., Beijing, Baoding, and

266   Shijiazhuang, the maximal mass concentration of $PM_{2.5}$ consistently exceed several hundred

267   µg m^{-3} during the polluted period. The $PM_{2.5}$ concentrations at the three megacities exhibit a

268   remarkable similarity in the timing and magnitude for the peak $PM_{2.5}$ concentrations. The

269   nearly synchronized temporal variations in the PM levels among the three megacities indicate

270   a prominent characteristic of severe haze formation, indicating the importance of *in-situ* PM

271   production over the entire region. During the evolution from clean, transition, to polluted

272   periods, the RH and wind speed is consistently increased and decreased, respectively (Fig. 1d).

273   The two polluted events on 28 September (EP1) and 5 October (EP2) are captured from

274   both *in-situ* measurements (Fig. 1) and satellite observations (Fig. 2). The satellite MODIS data

275   illustrate that the maximal AOD area occurs in the three megacities (i.e., BJ, BD, and SJZ). For

276   example, the AOD value in Beijing exceeds 4.0 and 2.0, during EP1 and EP2, respectively.

277   The spatial distribution of severe regional haze events is also depicted from the satellite visible

278   images, showing that a grey haze plume covers a substantial portion of the NCP region (Figs.

279   2c and d). The coincidence of the highest AOD areas with the locations of the megacities is

280   also discernable from the mean AOD values averaged over all the hazy days (e.g., daily $PM_{2.5}$ >

281   200 µg m^{-3}) in 2013 (Fig. S3), showing a large zone of elevated AOD values over the three

282   megacities. In contrast, the fall seasonal and annual AOD means averaged over all days in 2013

283   show that the maximal AOD values are located to the south of Beijing (Figs. 2e and f),

284   reflecting the typical regional transport pattens over this region (Guo et al., 2014; An et al.,2019;

285   Peng et al., 2021). In addition, the occurrence of severe haze events is consistently

286   accompanied by stagnant weather, characterized by weak southerly winds in Beijing and its

287   surrounding areas (Figs. 2a and b). For example, the wind speed is typically less than 1 m s^{-1}

288   in the highest AOD area (Figs. 2a and b), compared to that of a few to ten m s^{-1} during the clean

289   period (Fig. 1d). Air stagnation retards PM dispersion, resulting in minimal regional transport

290   during the polluted period. On the other hand, the gaseous aerosol precursors (e.g., SO_2, NO_x,

291   VOCs, and NH_3 with the chemical lifetimes from hours to days) are sufficiently transported

292   and dispersed prior to haze development over this region, as evident from much higher wind

293   speeds during the clean period (Fig. 1d). Efficient regional transport of the gaseous aerosol

294   precursors explains the similarity in the spatial/temporal PM variations, since well-mixed

295   gaseous aerosol precursors result in similar *in-situ* PM production under stagnant conditions

296   (Figs. 1a-c). Moreover, the coincidence of the AOD hotspots with the three megacities (Figs.

297   2a,b and S3) indicates more efficient *in-situ* PM production over the megacities, suggesting a

298   key role of traffic emissions (i.e., anthropogenic VOCs and NO_x) in facilitating regional severe

299   haze formation. While wind fluctuation likely results in PM variation in an isolated location,

300   especially for Beijing, which is situated at the northern edge of the NCP (Li et al. (2015), our

301   analysis of temporal/spatial PM distributions indicates that the dominant regional features

302   during the polluted period are reflected by rapid *in-situ* PM production and inefficient transport,

303   both of which are amplified by air stabilization.

304   **3.2. Photochemical PM formation**

305   To further elucidate the role of *in-situ* photochemical production in haze development,

306   we analyzed the temporally resolved PM properties in Beijing. Evidently, the $PM_{2.5}$ mass

307   concentration increases by more than 200 μg m^{-3} in less than 8 hrs. during the transition period

308   for EP1 and EP2 (Figs. 3a and b), which is dominated by the increase in the SOA mass

309   concentration linked to photochemical oxidation of VOCs (Guo et al., 2014; Liu et al., 2021).

310   The mass concentration of oxygenated organic aerosol (OOA) is typically considered as a

311   surrogate for SOA (Wood et al., 2010). Since OOA and the level of oxidants, O_x ($[O_x] \equiv$

312    $[O_3] + [NO_2]$), are both produced from oxidation of VOCs (Suh et al., 2001; Fan and Zhang,

313   2004; Zhao et al., 2005) and have a lifetime of longer than 12 hours, it is anticipated that both

314   quantities are correlated, when their formations occur on a similar timescale and at the same

315   location (Atkinson, 2000). Figs. 3a-d show that the increase in OOA is well correlated with the

316   O_x level during the transition period. The R^2 from linear regression between OOA and O_x

317   during the transition period (i.e., from 7:00 am to 2:30 pm) is 0.96 for EP1 and 0.95 for EP2

318   (Fig. 3e). The high correlation between OOA and O_x implies important *in-situ* production of

319   PM via photochemical reactions, consistent with the ground-based measurements (Fig. 1) and

320   satellite observations for PM (Fig. 2 and Fig. S3). The mean ratio of [OOA] to [O_x] for the two

321   episodes in Beijing is 0.34 ($\mu g\ m^{-3}\ ppb^{-1}$), suggesting highly efficient photochemistry. For

322   comparison, the mean ratio of [OOA] to [O_x] during the two episodes in Beijing is about 2.4

323   and 5.1 times of those in Mexico City and Houston (Wood et al., 2010), respectively, indicating

324   that the photochemical PM formation in Beijing is much more efficient than those in Mexico

325   City and Houston (Fig. 3f). The more efficient photochemical formation of PM in Beijing is

326   attributable to the presence of higher levels of anthropogenic aerosol precursors, such as

327   anthropogenic VOCs and NO_x, than those in the other two cities (Guo et al., 2014; Zhang et

328   al., 2015a). On the other hand, the correlation between [OOA] and [O_x] exists only during the

329   transition stage but vanishes during the polluted period. The latter is evident from the

330   continuing increase in [OOA] but decreasing [O_x]. In particular, O_3 production is significantly

331   suppressed during the polluted periods because of reduced solar ultraviolet radiation, leading

332   to inefficient photooxidation (Wu et al., 2020; Peng et al., 2021). Several previous studies have

333   attributed highly elevated levels of $PM_{2.5}$ during the polluted period to the importance of

334   multiphase chemistry to contribute to SIA and SOA formation (Wang et al., 2016; An et al.,

335   2019; Peng et al., 2021). For example, sulfate formation is effectively catalyzed by BC (Zhang

336   et al., 2020) and considerably enhanced via aqueous oxidation of SO_2 by NO_2 in the presence

337   of NH_3 during the transition/polluted periods (Wang et al., 2016), both increasing with

338   increasing RH. Also, oligomerization from dicarbonyls increases at high RH (Li et al., 2021a,

339   b), contributing to significantly enhanced SOA formation during the polluted periods (Zhang

340   et al., 2021).

14

3.3. Impacts of the haze-PBL interaction

3.3.1. A positive feedback of PM accumulation

To assess the impacts of haze-PBL interactions on PM pollution, we evaluated the correlation between the PM level and PBL height. Fig. 4 shows an analysis of daily mean PBL height versus $PM_{2.5}$ concentration between clean and hazy days from the ground-based measurements and the MERRA2 reanalysis data in 2013. The daily maximal PBL height is negatively correlated with surface $PM_{2.5}$ concentration (Fig. 4a). The diurnal cycle of the PBL height shows that the PBL height on severe haze days (daily $PM_{2.5}$ concentration > 200 μg m^{-3}) is significantly lower than that on clean days (daily $PM_{2.5}$ concentration < 30 μg m^{-3}), with a maximum difference of 800 m (Fig. 4b). Furthermore, the dimming area over NCP, which is reflected by the lower mean of the satellite-retrieved surface solar radiation (SSR) averaged over all the severe haze days in 2013, coincides with the region with the highest AOD (Fig. S3), implying a strong spatial association between the solar radiation intensity and PM pollution at the surface. The co-locations in the areas between the lowest SSR and highest AOD also reflects the occurrence of the highest PM levels at the megacities during the regional severe haze episodes.

We further elucidated the response of PBL development to the PM pollution, and the linkage between the aerosol-PBL interactions and aerosol radiative effects are further elucidated by performing sensitivity modeling studies on the two hazy days (Figs. 5-6). The performance of the model simulations was validated by comparison with field observations. The simulated temperature and RH are consistent with the sounding data in light of the vertical variations (Fig. S2). The simulated AOD at 550 nm is 0.05 and 3.6 on 25 and 28 September 2013 for EP1, respectively, and 0.04 and 2.0 on 2 and 5 October 2013 for EP2, respectively, in qualitative agreement with the Aerosol Robotic Network (AERONET) measurements in Beijing (Table 2). The simulated one-day accumulated surface solar radiation and the peak

366   solar radiation flux in the aged-BC case for EP1 (EP2) are 9.2 MJ m^{-2} (11.3 MJ m^{-2}) and 326

367   W m^{-2} (402 W m^{-2}), respectively, comparable to the ground-based measurement of 10.6 MJ m^{-2}

368   ^{2} (9.8 MJ m^{-2}) and 408 W m^{-2} (452 W m^{-2}) in Table 2. The temporal evolutions of PBL and its

369   peak heights derived from the aged-BC cases are also consistent with the available

370   measurements (Figs. 5a and g).

371   The simulated maximal height of PBL under the polluted condition is reduced by more

372   than 300 m relative to the clean condition (Figs. 5a and g). The reduction in PBL height is

373   explained by the aerosol radiative effects. Under the polluted condition, a warmer temperature

374   is located at the altitude of around 1.2 km, and less SSR reaches the ground level (Figs. 5e and

375   k, f and l). Also, the surface temperature is reduced by several degrees (Figs. 5e and k, and

376   Figs. 6a and c). Consequently, the turbulent kinetic energy (TKE) is reduced, and the updraft

377   is weakened in the aged-BC cases relative to the clean cases (Figs. 5b, c, h and i), leading to an

378   enhanced atmospheric stratification and hindered development of PBL. The largely reduced

379   TKE during the polluted periods from the model simulations is consistent with field

380   measurements, showing that the turbulent fluxes are greatly reduced in the mixed surface layer

381   under polluted conditions (Wilcox et al., 2016). In addition, surface winds are reduced by 0.7

382   m s^{-1} from clean to aged-BC cases (Fig. 6b and d), leading to suppressed entrainment aloft and

383   restricted development of the PBL.

384   The interaction between aerosols and PBL induces further feedbacks at the surface by

385   altering atmospheric dynamic/thermodynamic conditions and stability. For example, the PM

386   concentration at the ground level accumulates when the PBL is compressed, resulting in a

387   smaller extent for vertical dilution. Also, the diurnal feature of PM pollution diminishes

388   because of collapsed PBL, allowing PM to continuously accumulate at the surface. In addition,

389   horizontal advection is also suppressed under polluted conditions, as reflected by weak wind

390   speeds. Consequently, the heavy haze period persists over an extensive period (about 4-7 days)

Atmospheric
Chemistry
and Physics
Discussions

391   over this region and is only dissipated by strongly northly winds associated with frontal passage

392   (Guo et al., 2014; An et al., 2019). The continuous PM accumulation for multiple days over

393   the NCP is distinct from other megacities across the world, such as Houston, Los Angeles, and

394   Mexico City, which always exhibit a clear diurnal feature of the PM levels (Zhang et al., 2015a),

395   implying a key role of the haze-PBL interaction in deteriorating air quality and worsening the

396   hazy condition in this region.

397   The suppression in PBL height results in significant enhancement of atmospheric

398   moisture, another crucial factor affects the haze evolution, which promotes the occurrence of

399   multiphase reactions (Li et al., 2021a, b). The measured RH increases greatly during the two

400   episodes (Fig. 1d), i.e., from about 18%-19% on the clean days (25 September and 2 October)

401   to 53%-55% on the polluted days (28 September and 5 October). To evaluate the sensitivity of

402   the atmospheric moisture to the PBL height, we employed a modified Nozaki's equation

403   (Nozaki, 1973; Tie et al., 2017) to calculate the RH under different PBL height scenarios using

404   the observed meteorological conditions as inputs (Table 3). The calculated RH increases from

405   19% to 68% for EP1 and from 21% to 73% for EP2, when the PBL height decreased by about

406   1000 m during the polluted days, indicating that the humidity is highly sensitive to the PBL

407   height.

408   The elevated RH during the polluted period is explained from collapsed PBL to inhibit

409   vertical moisture transport, reduced surface temperature leading to lower saturation vapor

410   pressure, and inefficient entrainment of dry air aloft (Fan et al., 2008; Liu et al., 2013). In

411   addition, enhanced moisture leads to hygroscopic growth of aerosol particles (Liu et al., 2013;

412   Tie et al., 2017). For example, the growth hygroscopic factor relevant to the RH enhancement

413   during EP1 and EP2 increases from 1.3 on the clean days to 1.5 on the hazy days, using an

414   empirical equation derived according to Meier et al. (2009). The additional aerosol growth

415   causes additional attenuation of incoming solar radiation by scattering and absorption to

416   amplify PBL suppression. Moreover, an enlarged aerosol surface area (due to hygroscopic

417   growth) and elevated RH during the polluted periods favor aqueous-phase reactions to produce

418   sulfate, nitrate, and SOA (Wang et al., 2016a). For example, a recent experimental/field study

419   has shown enhanced sulfate formation, which is catalyzed by BC and increases monotonically

420   from 10% to 70% RH (Zhang et al., 2020). Also, the aqueous reaction of dicarbonyls, which

421   are produced with high yields from oxidation of aromatic VOCs, is significantly enhanced at

422   high RH to yield oligemic products and enhance SOA formation (Li et al., 2021a; b). Hence,

423   enhanced PM production near the ground level strengthens the suppressing effect for the PBL

424   development and results in stabilization and moisture enhancement, constituting positive

425   feedback to amplify the haze development.

3.3.3. The BC effects

426

427   We performed model sensitivity simulations to elucidate the role of BC in PBL

428   suppression by considering the non-BC, fresh-BC, and aged-BC scenarios during the polluted

429   periods. Comparison shows a negligible effect on the haze-PBL interaction between the non-

430   BC and fresh-BC cases (Figs. 5, 6 and S4) but large changes in solar radiation and

431   thermodynamic/dynamic conditions within the PBL between the non-BC/ fresh-BC and aged-

432   BC cases, which are attributed to the radiative effects of aged BC. For example, the shortwave

433   heating rate per unit mass is much larger for aged-BC than non-BC and is two times higher for

434   aged-BC than fresh-BC (Figs. 5d and j), suggesting that the BC aging process greatly attenuate

435   incoming solar radiation. Although BC accounts for only 6% of the total aerosol mass under

436   the polluted conditions, about one third of the total reduction in SSR for full-component

437   aerosols is attributed to absorption enhancement after BC aging (Figs. 5f and l). The reduced

438   SSR by the BC aging leads to a cooling of 0.5-0.8 K at the surface. As a result, BC aging

439   contributes significantly to atmospheric stabilization, as evident from weaker updrafts, smaller

440   TKE, and shallower PBL for the aged-BC case (Fig. 5).

441   The BC aging causes a decrease in the maximum PBL height (at noontime) by about

442   150 m for the aged-BC case compared to the non-BC and fresh-BC cases. Overall, the BC

443   aging contributes more than 30% of the total reduction in the PBL height by all aerosol

444   components. The restricted PBL development by BC absorption in our work is consistent with

445   that identified previously (Ding et al., 2016; Petäjä et al., 2016). Using a radiative transfer

446   model, Zhang et al. (2020) shows large strongly positive radiative forcing in the atmosphere

447   and strongly negative radiative forcing at the surface by BC aging, consistent with those of the

448   maximal estimates at about noontime from our calculations (Fig. 5i,f).

449   **3.5. Aerosol direct radiative forcing**

450   The aerosol direct radiative forcing during regional haze also exhibits a profound

451   climatic effect (Ramanathan et al., 2007). Fig. 7 shows that the total aerosol radiative forcing

452   at the surface (SFC) and in the atmosphere (ATM) during the haze episodes EP1 (EP2) are -

453   87.8 (-62.8) W m^{-2} and 82.2 (56.9) W m^{-2}, respectively. The positive radiative forcing by all

454   aerosols in the atmosphere is dominated by that of aged BC, which accounts for 80% of the

455   total radiative forcing for both episodes. The net radiative forcing at the top of the atmosphere

456   (TOA) by all aerosols for EP1 (EP2) is around -5.6 (-5.9) W m^{-2}, much smaller than the non-

457   BC case with a large negative value of -36.8 (-26.0) W m^{-2}. The strong cooling at the surface

458   is largely canceled out by the strong warming in the atmosphere under the polluted condition,

459   leading to a small net TOA forcing. Clearly, BC aging contributes significantly to cooling at

460   the surface and warming aloft and, hence, the overall radiative budget during the polluted

461   periods. Climatologically, the aerosol TOA forcing on the regional/national level has been

462   shown to be nearly zero or slightly positive in China (Li et al., 2007; Ramanathan et al., 2007;

463   Ding et al., 2016), also demonstrating that the large positive forcing by absorbing aerosols

464   greatly compensates the negative forcing by the non-absorbing aerosols (Table S1). Therefore,

465   regional global warming is likely mitigated by reducing BC emissions (Wang et al., 2015b).

19

466 **4. Conclusions**

467   In this work, we analyzed the temporal and spatial characteristics of PM pollution

468 during severe haze events over NCP, by examining ground-based measurements and satellite

469 observations. Severe haze occurs frequently over this region, evident from a periodic (4-7 days)

470 cycle of highly elevated PM pollution. The PM evolutions among the three megacities (Beijing,

471 Baoding and Shijiazhuang) exhibit a remarkable similarity during the haze events, showing

472 nearly synchronized temporal variations in the PM levels. The similar timing and magnitude

473 in the peak $PM_{2.5}$ concentrations among the three megacities indicate significant *in-situ* PM

474 production. Satellite measurements show that the AOD hotspots during the polluted period are

475 co-located with the three megacities, but are distinct from seasonal and annual AOD means,

476 indicating the importance of urban emissions (mainly traffic emissions consisting of

477 anthropogenic VOCs and NO_x). *In-situ* PM production occurs most efficiently over the

478 megacities, and urban sources relevant to traffic emissions play a critical role in regional severe

479 haze formation.

480   Our result reveals that the rapid photochemistry drives the PM production during the

481 transition period. There exist concurrent increases in OOA and $PM_{2.5}$ concentrations and a

482 strong correlation between OOA and O_x concentrations during this period. The [OOA]/[Ox]

483 ratio in Beijing is much higher than that in Mexico City and Houston, attributable to much

484 higher level of gaseous precursors (i.e., anthropogenic VOCs and NO_x) in Beijing than the

485 other two cities. The correlation between [OOA] and [O_x], however, vanishes during the

486 polluted period, when O_3 production is significantly suppressed because of reduced solar

487 ultraviolet radiation and inefficient photooxidation (Wu et al., 2020; Peng et al., 2021). The

488 continuing increases in $PM_{2.5}$ and OOA with decreasing O_x during the polluted period implies

489 a key role of multiphase chemistry in driving the haze severity, when the RH level is

490 significantly elevated. The continuous growth in $PM_{2.5}$ and OOA during the polluted period

491 has been explained by an increasing importance of heterogeneous chemistry to contribute to

492 sulfate, nitrate, and SOA formation (Wang et al., 2016a; An et al., 2019; Peng et al., 2021;

493 Zhang et al., 2021).

494 Using the WRF model coupled with an explicit aerosol radiative module, we elucidated

495 the underlying mechanism relevant to the haze-PBL interactions, showing a positive feedback

496 to haze formation at the ground level. The PBL height is largely reduced under the polluted

497 condition, since the PBL is markedly suppressed (as indicated by the reduced TKE and

498 weakened updraft), because of strong aerosol heating in the atmosphere and strong cooling at

499 the surface. The PM concentration near the surface accumulates significantly in a compressed

500 PBL, since PM dispersion is unfavorable in the stratified and collapsed PBL, leading to

501 continuous growth and accumulation of PM over multiple days. Calculations using the

502 modified Nozaki's equation shows that the suppressed PBL results in a great enhancement of

503 atmospheric moisture near the surface. A more humid condition leads to hygroscopic growth

504 of aerosol particles and more efficient multiphase PM production. Therefore, haze development

505 near the surface is considerably exacerbated because of the positive feedback in responding to

506 the atmospheric moisture and thermodynamic/dynamic conditions to amplify the haze severity.

507 Our combined observational analysis of the temporal/spatial PM distributions and

508 modeling unravel a dominant regional characteristic for severe haze evolution in the NCP

509 region, showing rapid *in-situ* PM production and inefficient transport, both of which are

510 amplified by air stabilization. On the other hand, regional transport sufficiently disperses the

511 gaseous aerosol precursors (SO_2, NO_x, VOCs, and NH_3) during the clean period, which

512 subsequently result in rapid *in-situ* PM production via photochemistry during the transition

513 period and via multiphase chemistry during the polluted period.

514 The modeling simulations on two haze episodes indicate important regional climatic

515 effects. The net TOA forcing for the two hazy days is about of -5.6 ~ -5.9 W m^{-2}, showing

Atmospheric
Chemistry
and Physics
Discussions
Open Access
EGU

516   strong negative radiative forcing (cooling) of -63 to -88 W m^{-2} at the surface and strong positive

517   radiative forcing (warming) of 57 to 82 W m^{-2} in the atmosphere. BC represents the dominant

518   contributor to the positive aerosol radiative forcing in the atmosphere, thus playing a significant

519   role in the haze-PBL interaction. Specifically, BC aging contributes to more than 30% of the

520   PBL collapse induced by total aerosols and about 50% of the TOA positive radiative forcing.

521   Our work highlights the necessity to better understand the BC aging process and improve

522   representation in atmospheric models for accurate assessment of the aerosol climatic effects.

523   We conclude that reduction in BC emissions achieves co-benefits, which improve local and

524   regional air quality by minimizing air stagnation and mitigate the global warming by alleviating

525   the positive direct radiative forcing.

532

533 **References**

534 An, Z. S., Huang, R. J., Zhang, R. Y., Tie, X. X., Li, G. H., Cao, J. J., Zhou, W. J., Shi, Z. G.,

535   Han, Y. M., Gu, Z. L., and Ji, Y. M.: Severe haze in northern China: A synergy of

536   anthropogenic emissions and atmospheric processes, Proc. Natl. Acad. Sci. USA, 116,

537   8657-8666, 10.1073/pnas.1900125116, 2019.

538 Atkinson, R.: Atmospheric chemistry of VOCs and NOx, Atmos. Environ., 34, 2063-2101,

539   http://dx.doi.org/10.1016/S1352-2310(99)00460-4, 2000.

540 Bond, T. C., Doherty, S. J., Fahey, D. W., Forster, P. M., Berntsen, T., DeAngelo, B. J.,

541   Flanner, M. G., Ghan, S., Kärcher, B., Koch, D., Kinne, S., Kondo, Y., Quinn, P. K.,

542   Sarofim, M. C., Schultz, M. G., Schulz, M., Venkataraman, C., Zhang, H., Zhang, S.,

543   Bellouin, N., Guttikunda, S. K., Hopke, P. K., Jacobson, M. Z., Kaiser, J. W., Klimont,

544   Z., Lohmann, U., Schwarz, J. P., Shindell, D., Storelvmo, T., Warren, S. G., and Zender,

545   C. S.: Bounding the role of black carbon in the climate system: A scientific assessment, J.

546   Geophys. Res.: Atmos., 118, 5380-5552, 10.1002/jgrd.50171, 2013.

547 Bouarar, I., Wang, X. M., and Brasseur, G. P.: Air Pollution in Eastern Asia: An Integrated

548   Perspective Preface, Issi Sci Rep Ser, 16, V-Viii, Book_Doi 10.1007/978-3-319-59489-7,

549   2017.

550 Cai, W., Li, K., Liao, H., Wang, H., and Wu, L.: Weather conditions conducive to Beijing

551   severe haze more frequent under climate change, Nature Clim. Change, 7, 257,

552   10.1038/nclimate3249, 2017.

553 Che, H., Xia, X., Zhu, J., Li, Z., Dubovik, O., Holben, B., Goloub, P., Chen, H., Estelles, V.,

554   Cuevas-Agullo, E., Blarel, L., Wang, H., Zhao, H., Zhang, X., Wang, Y., Sun, J., Tao, R.,

555   Zhang, X., and Shi, G.: Column aerosol optical properties and aerosol radiative forcing

556   during a serious haze-fog month over North China Plain in 2013 based on ground-based

557   sunphotometer measurements, Atmos. Chem. Phys., 14, 2125-2138, 10.5194/acp-14-

558   2125-2014, 2014.

559   Ding, A. J., Huang, X., Nie, W., Sun, J. N., Kerminen, V. M., Petäjä, T., Su, H., Cheng, Y.

560   F., Yang, X. Q., Wang, M. H., Chi, X. G., Wang, J. P., Virkkula, A., Guo, W. D., Yuan,

561   J., Wang, S. Y., Zhang, R. J., Wu, Y. F., Song, Y., Zhu, T., Zilitinkevich, S., Kulmala,

562   M., and Fu, C. B.: Enhanced haze pollution by black carbon in megacities in China,

563   Geophys. Res. Lett., 43, 2873–2879, 10.1002/2016GL067745, 2016.

564   Fan, J., and Zhang, R. Atmospheric oxidation mechanism of isoprene. Environ. Chem., 1,

565   140-149, 2004.

566   Fan, J., Zhang, R., Tao, W.-K., and Mohr, K. I.: Effects of aerosol optical properties on deep

567   convective clouds and radiative forcing, J. Geophys. Res., 113, D08209,

568   10.1029/2007jd009257, 2008.

569   Guo, S., Hu, M., Zamora, M. L., Peng, J., Shang, D., Zheng, J., Du, Z., Wu, Z., Shao, M.,

570   Zeng, L., Molina, M. J., and Zhang, R.: Elucidating severe urban haze formation in

571   China, Proc. Natl. Acad. Sci. U S A, 111, 17373-17378, 10.1073/pnas.1419604111, 2014.

572   Guo, S., Hu, M., Peng, J. F., Wu, Z. J., Zamora, M. L., Shang, D. J., Du, Z. F., Zheng, J.,

573   Fang, X., Tang, R. Z., Wu, Y. S., Zeng, L. M., Shuai, S. J., Zhang, W. B., Wang, Y., Ji,

574   Y. M., Li, Y. X., Zhang, A. L., Wang, W. G., Zhang, F., Zhao, J. Y., Gong, X. L., Wang,

575   C. Y., Molina, M. J., and Zhang, R. Y.: Remarkable nucleation and growth of ultrafine

576   particles from vehicular exhaust, Proc. Natl. Acad. Sci. USA, 117, 3427-3432,

577   10.1073/pnas.1916366117, 2020.

578   Guo, S., Hu, M., Lin, Y., Gomez-Hernandez, M., Zamora, M. L., Peng, J. F., Collins, D. R.,

579   and Zhang, R. Y.: OH-Initiated Oxidation of m-Xylene on Black Carbon Aging, Environ.

580   Sci. Technol., 50, 8605-8612, 10.1021/acs.est.6b01272, 2016.

581   Gustafsson, Ö., and Ramanathan, V.: Convergence on climate warming by black carbon

582   aerosols, Proc. Natl. Acad. Sci. USA, 113, 4243-4245, 10.1073/pnas.1603570113, 2016.

583   He, C., Liou, K. N., Takano, Y., Zhang, R., Levy Zamora, M., Yang, P., Li, Q., and Leung, L.

584   R.: Variation of the radiative properties during black carbon aging: theoretical and

585   experimental intercomparison, Atmos. Chem. Phys., 15, 11967-11980, 10.5194/acp-15-

586   11967-2015, 2015.

587   Intergovernmental Panel on Climate Change (IPCC). *Climate Change 2013: The Physical*

588   *Science Basis. Contribution of Working Group I to the Fifth Assessment Report of the*

589   *Intergovernmental Panel on Climate Change*. Cambridge University Press, **2013**.

590   Khalizov, A. F., Lin, Y., Qiu, C., Guo, S., Collins, D., and Zhang, R.: Role of OH-initiated

591   oxidation of isoprene in aging of combustion soot, Environ. Sci. Technol., 47, 2254-2263,

592   10.1021/es3045339, 2013.

593   Johnson, N. M., Hoffmann, A. R., Behlen, J. C., Lau, C., Pendleton, D., Harvey, N., Shore,

594   R., Li, Y. X., Chen, J. S., Tian, Y. A., and Zhang, R. Y.: Air pollution and children's

595   health-a review of adverse effects associated with prenatal exposure from fine to ultrafine

596   particulate matter, Environ. Health. Prev., 26, ARTN 72, 10.1186/s12199-021-00995-5,

597   2021.

598   Levy, R. C., Leptoukh, G. G., Kahn, R., Zubko, V., Gopalan, A., and Remer, L. A.: A

599   Critical Look at Deriving Monthly Aerosol Optical Depth From Satellite Data, Ieee T

600   Geosci Remote, 47, 2942-2956, Doi 10.1109/Tgrs.2009.2013842, 2009.

601   Li, G., Wang, Y., and Zhang, R.: Implementation of a two-moment bulk microphysics

602   scheme to the WRF model to investigate aerosol-cloud interaction, J. Geophys. Res., 113,

603   D15211, 10.1029/2007jd009361, 2008.

604   Li, P., Yan, R., Yu, S., Wang, S., Liu, W., and Bao, H.: Reinstate regional transport of PM2.5

605   as a major cause of severe haze in Beijing, Proc. Natl. Acad. Sci. USA, 112, E2739-

606   E2740, 10.1073/pnas.1502596112, 2015.

607   Li, Y., Zhao, J., Wang, Y., Seinfeld, J. H., and Zhang, R.: Multigeneration Production of

608   Secondary Organic Aerosol from Toluene Photooxidation, Environmental science &

609   technology, 55, 8592-8603, 10.1021/acs.est.1c02026, 2021a.

610   Li, Y., Ji, Y., Zhao, J., Wang, Y., Shi, Q., Peng, J., Wang, Y., Wang, C., Zhang, F., Wang,

611   Y., Seinfeld, J. H., and Zhang, R.: Unexpected Oligomerization of Small α-Dicarbonyls

612   for Secondary Organic Aerosol and Brown Carbon Formation, Environmental science &

613   technology, 55, 4430-4439, 10.1021/acs.est.0c08066, 2021b.

614   Li, Z., Xia, X., Cribb, M., Mi, W., Holben, B., Wang, P., Chen, H., Tsay, S.-C., Eck, T. F.,

615   Zhao, F., Dutton, E. G., and Dickerson, R. E.: Aerosol optical properties and their

616   radiative effects in northern China, J. Geophys. Res.: Atmos., 112, D22S01,

617   10.1029/2006JD007382, 2007.

618   Li, Z., Guo, J., Ding, A., Liao, H., Liu, J., Sun, Y., Wang, T., Xue, H., Zhang, H., and Zhu,

619   B.: Aerosol and Boundary-Layer Interactions and Impact on Air Quality, Natl. Sci. Rev.,

620   nwx117-nwx117, 10.1093/nsr/nwx117, 2017.

621   Li, Z. Q., Wang, Y., Guo, J. P., Zhao, C. F., Cribb, M., Dong, X. Q., Fan, J. W., Gong, D. Y.,

622   Huang, J. P., Jiang, M. J., Jiang, Y. Q., Lee, S. S., Li, H., Li, J. M., Liu, J. J., Qian, Y.,

623   Rosenfeld, D., Shan, S. Y., Sun, Y. L., Wang, H. J., Xin, J. Y., Yan, X., Yang, X., Yang,

624   X. Q., Zhang, F., and Zheng, Y. T.: East Asian Study of Tropospheric Aerosols and their

625   Impact on Regional Clouds, Precipitation, and Climate (EAST-AIR(CPC)), J. Geophys.

626   Res.-Atmos., 124, 13026-13054, 10.1029/2019jd030758, 2019.

627 Lin, Y., Wang, Y., Pan, B., Hu, J., Liu, Y., and Zhang, R.: Distinct Impacts of Aerosols on an

628   Evolving Continental Cloud Complex during the RACORO Field Campaign, J. Atmos.

629   Sci., 73, 3681-3700, doi:10.1175/JAS-D-15-0361.1, 2016.

630 Liu, J., F. Zhang, W. Xu, Y. Sun, L. Chen, S. Li, J. Ren, B. Hu, H. Wu, and R. Zhang,

631   Hygroscopicity of organic aerosols linked to formation mechanisms. Geophy. Res. Lett.

632   48, doi.org/10.1029/2020GL091683, 2021.

633 Liu, X. G., Li, J., Qu, Y., Han, T., Hou, L., Gu, J., Chen, C., Yang, Y., Liu, X., Yang, T.,

634   Zhang, Y., Tian, H., and Hu, M.: Formation and evolution mechanism of regional haze: a

635   case study in the megacity Beijing, China, Atmos. Chem. Phys., 13, 4501-4514, DOI

636   10.5194/acp-13-4501-2013, 2013.

637 Mallet, M., Roger, J. C., Despiau, S., Putaud, J. P., and Dubovik, O.: A study of the mixing

638   state of black carbon in urban zone, J. Geophys. Res.: Atmos., 109, n/a-n/a,

639   10.1029/2003JD003940, 2004.

640 Meier, J., Wehner, B., Massling, A., Birmili, W., Nowak, A., Gnauk, T., Brüggemann, E.,

641   Herrmann, H., Min, H., and Wiedensohler, A.: Hygroscopic growth of urban aerosol

642   particles in Beijing (China) during wintertime: a comparison of three experimental

643   methods, Atmos. Chem. Phys., 9, 6865-6880, 10.5194/acp-9-6865-2009, 2009.

644 Menon, S., Hansen, J., Nazarenko, L., and Luo, Y.: Climate Effects of Black Carbon

645   Aerosols in China and India, Science, 297, 2250-2253, 10.1126/science.1075159, 2002.

646 Molina, L. T.: Introductory lecture: air quality in megacities, Faraday Discuss, 226, 9-52,

647   10.1039/d0fd00123f, 2021.

648 Nozaki, K. Y.: Mixing Depth Model Using Hourly Surface Observations Report 7053, USAF

649   Environmental Technical Applications Center, 1973.

650 Pasquill, F.: The Estimation of the Dispersion of Windborne Material, Meteorological

651   Magazin, 90, 33-49, 1961.

27

652   Peng, J., Hu, M., Guo, S., Du, Z., Zheng, J., Shang, D., Levy Zamora, M., Zeng, L., Shao,

653   M., Wu, Y.-S., Zheng, J., Wang, Y., Glen, C. R., Collins, D. R., Molina, M. J., and

654   Zhang, R.: Markedly enhanced absorption and direct radiative forcing of black carbon

655   under polluted urban environments, Proc. Natl. Acad. Sci. USA, 4266–4271,

656   10.1073/pnas.1602310113, 2016.

657   Peng, J., Hu, M., Guo, S., Du, Z., Shang, D., Zheng, J., Zheng, J., Zeng, L., Shao, M., Wu,

658   Y., Collins, D., and Zhang, R.: Ageing and hygroscopicity variation of black carbon

659   particles in Beijing measured by a quasi-atmospheric aerosol evolution study

660   (QUALITY) chamber, Atmos. Chem. Phys., 17, 10333-10348, 10.5194/acp-17-10333-

661   2017, 2017.

662   Peng, J. F., Hu, M., Shang, D. J., Wu, Z. J., Du, Z. F., Tan, T. Y., Wang, Y. N., Zhang, F.,

663   and Zhang, R. Y.: Explosive Secondary Aerosol Formation during Severe Haze in the

664   North China Plain, Environ. Sci. Technol., 55, 2189-2207, 10.1021/acs.est.0c07204,

665   2021.

666   Petäjä, T., Järvi, L., Kerminen, V. M., Ding, A. J., Sun, J. N., Nie, W., Kujansuu, J.,

667   Virkkula, A., Yang, X., Fu, C. B., Zilitinkevich, S., and Kulmala, M.: Enhanced air

668   pollution via aerosol-boundary layer feedback in China, Sci. Rep., 6, 18998,

669   10.1038/srep18998, 2016.

670   Qian, Y., Leung, R.L., Ghan, S. J., and Giorgi, F.: Regional climate effects of aerosols over

671   China: modeling and observation, Tellus B, 55, 914-934, 10.1046/j.1435-

672   6935.2003.00070.x, 2003.

673   Qian, Y, Gong, D., Fan, J., Leung, R.L., Bennartz, R., Chen, D., Wang, W.: Heavy pollution

674   suppresses light rain in China: Observations and modeling, J. Geophys. Res.: Atmos.,

675   114, 10.1029/2008JD011575, 2009.

676   Ramanathan, V., Li, F., Ramana, M. V., Praveen, P. S., Kim, D., Corrigan, C. E., Nguyen, H.,

677   Stone, E. A., Schauer, J. J., Carmichael, G. R., Adhikary, B., and Yoon, S. C.:

678   Atmospheric brown clouds: Hemispherical and regional variations in long-range

679   transport, absorption, and radiative forcing, J. Geophys. Res.: Atmos., 112, D22S21,

680   10.1029/2006JD008124, 2007.

681   Rychlik, K. A., Secrest, J. R., Lau, C., Pulczinski, J., Zamora, M. L., Leal, J., Langley, R.,

682   Myatt, L. G., Raju, M., Chang, R. C. A., Li, Y. X., Golding, M. C., Rodrigues-Hoffmann,

683   A., Molina, M. J., Zhang, R. Y., and Johnson, N. M.: In utero ultrafine particulate matter

684   exposure causes offspring pulmonary immunosuppression, Proc. Natl. Acad. Sci. USA,

685   116, 3443-3448, 10.1073/pnas.1816103116, 2019.

686   Suh, I., Lei, W., and Zhang, R. Experimental and theoretical studies of isoprene reaction with

687   NO_3. J. Phys. Chem. 105, 6471-6478, 2001.

688   Sun, Y. L., Jiang, Q., Wang, Z. F., Fu, P. Q., Li, J., Yang, T., and Yin, Y.: Investigation of

689   the Sources and Evolution Processes of Severe Haze Pollution in Beijing in January 2013,

690   J. Geophys Res.-Atmos., 119, 4380-4398, Doi 10.1002/2014jd021641, 2014.

691   Tang, G., Zhang, J., Zhu, X., Song, T., Münkel, C., Hu, B., Schäfer, K., Liu, Z., Zhang, J.,

692   Wang, L., Xin, J., Suppan, P., and Wang, Y.: Mixing layer height and its implications for

693   air pollution over Beijing, China, Atmos. Chem. Phys., 16, 2459-2475, 10.5194/acp-16-

694   2459-2016, 2016a.

695   Tang, W., Qin, J., Yang, K., Liu, S., Lu, N., and Niu, X.: Retrieving high-resolution surface

696   solar radiation with cloud parameters derived by combining MODIS and MTSAT data,

697   Atmos. Chem. Phys., 16, 2543-2557, 10.5194/acp-16-2543-2016, 2016b.

698   Tie, X., Huang, R.-J., Cao, J., Zhang, Q., Cheng, Y., Su, H., Chang, D., Pöschl, U.,

699   Hoffmann, T., Dusek, U., Li, G., Worsnop, D. R., and O'Dowd, C. D.: Severe Pollution

700   in China Amplified by Atmospheric Moisture, Sci. Rep., 7, 15760, 10.1038/s41598-017-

701   15909-1, 2017.

702   Wallace, J. M., and Hobbs, P. V.: Atmospheric Science, Second Edition, Elsevier, 2005.

703   Wang, G., Zhang, R., Gomez, M. E., Yang, L., Levy Zamora, M., Hu, M., Lin, Y., Peng, J.,

704   Guo, S., Meng, J., Li, J., Cheng, C., Hu, T., Ren, Y., Wang, Y., Gao, J., Cao, J., An, Z.,

705   Zhou, W., Li, G., Wang, J., Tian, P., Marrero-Ortiz, W., Secrest, J., Du, Z., Zheng, J.,

706   Shang, D., Zeng, L., Shao, M., Wang, W., Huang, Y., Wang, Y., Zhu, Y., Li, Y., Hu, J.,

707   Pan, B., Cai, L., Cheng, Y., Ji, Y., Zhang, F., Rosenfeld, D., Liss, P. S., Duce, R. A.,

708   Kolb, C. E., and Molina, M. J.: Persistent sulfate formation from London Fog to Chinese

709   haze, Proc. Natl. Acad. Sci. USA, 113, 13630-13635, 10.1073/pnas.1616540113, 2016a.

710   Wang, H., Shi, G. Y., Zhang, X. Y., Gong, S. L., Tan, S. C., Chen, B., Che, H. Z., and Li, T.:

711   Mesoscale modelling study of the interactions between aerosols and PBL meteorology

712   during a haze episode in China Jing–Jin–Ji and its near surrounding region – Part 2:

713   Aerosols' radiative feedback effects, Atmos. Chem. Phys., 15, 3277-3287, 10.5194/acp-

714   15-3277-2015, 2015a.

715   Wang, J., Allen, D. J., Pickering, K. E., Li, Z., and He, H.: Impact of aerosol direct effect on

716   East Asian air quality during the EAST-AIRE campaign, J. Geophys. Res.: Atmos., 121,

717   6534-6554, 10.1002/2016JD025108, 2016b.

718   Wang, Y., Wan, Q., Meng, W., Liao, F., Tan, H., and Zhang, R.: Long-term impacts of

719   aerosols on precipitation and lightning over the Pearl River Delta megacity area in China,

720   Atmos. Chem. Phys., 11, 12421-12436, 10.5194/acp-11-12421-2011, 2011.

721   Wang, Y., Che, H., Ma, J., Wang, Q., Shi, G., Chen, H., Goloub, P., and Hao, X.: Aerosol

722   radiative forcing under clear, hazy, foggy, and dusty weather conditions over Beijing,

723   China, Geophys. Res. Lett., 36, n/a-n/a, 10.1029/2009GL037181, 2009.

724   Wang, Y., Khalizov, A., Levy, M., and Zhang, R. Y.: New Directions: Light absorbing

725   aerosols and their atmospheric impacts, Atmos. Environ., 81, 713-715,

726   10.1016/j.atmosenv.2013.09.034, 2013.

727   Wang, Y., Zhang, R., and Saravanan, R.: Asian pollution climatically modulates mid-latitude

728   cyclones following hierarchical modelling and observational analysis, Nat. commun., 5,

729   3098, 10.1038/ncomms4098, 2014a.

730   Wang, Y., Wang, M., Zhang, R., Ghan, S. J., Lin, Y., Hu, J., Pan, B., Levy, M., Jiang, J. H.,

731   and Molina, M. J.: Assessing the effects of anthropogenic aerosols on Pacific storm track

732   using a multiscale global climate model, Proc. Natl. Acad. Sci. U S A, 111, 6894-6899,

733   10.1073/pnas.1403364111, 2014b.

734   Wang, Y., Lee, K.-H., Lin, Y., Levy, M., and Zhang, R.: Distinct effects of anthropogenic

735   aerosols on tropical cyclones, Nature Clim. Change, 4, 368-373, 10.1038/nclimate2144,

736   2014c.

737   Wang, Y. S., Yao, L., Wang, L. L., Liu, Z. R., Ji, D. S., Tang, G. Q., Zhang, J. K., Sun, Y.,

738   Hu, B., and Xin, J. Y.: Mechanism for the Formation of the January 2013 Heavy Haze

739   Pollution Episode over Central and Eastern China, Sci. China Earth Sci., 57, 14-25, DOI

740   10.1007/s11430-013-4773-4, 2014d.

741   Wang, Z., Huang, X., and Ding, A.: Dome effect of black carbon and its key influencing

742   factors: A one-dimensional modelling study, Atmos. Chem. Phys. Discuss., 2017, 1-29,

743   10.5194/acp-2017-967, 2017.

744   Wang, Z. L., Zhang, H., and Zhang, X. Y.: Simultaneous reductions in emissions of black

745   carbon and co-emitted species will weaken the aerosol net cooling effect, Atmos. Chem.

746   Phys., 15, 3671-3685, 10.5194/acp-15-3671-2015, 2015b.

747   Wilcox, E. M., Thomas, R. M., Praveen, P. S., Pistone, K., Bender, F. A.-M., and

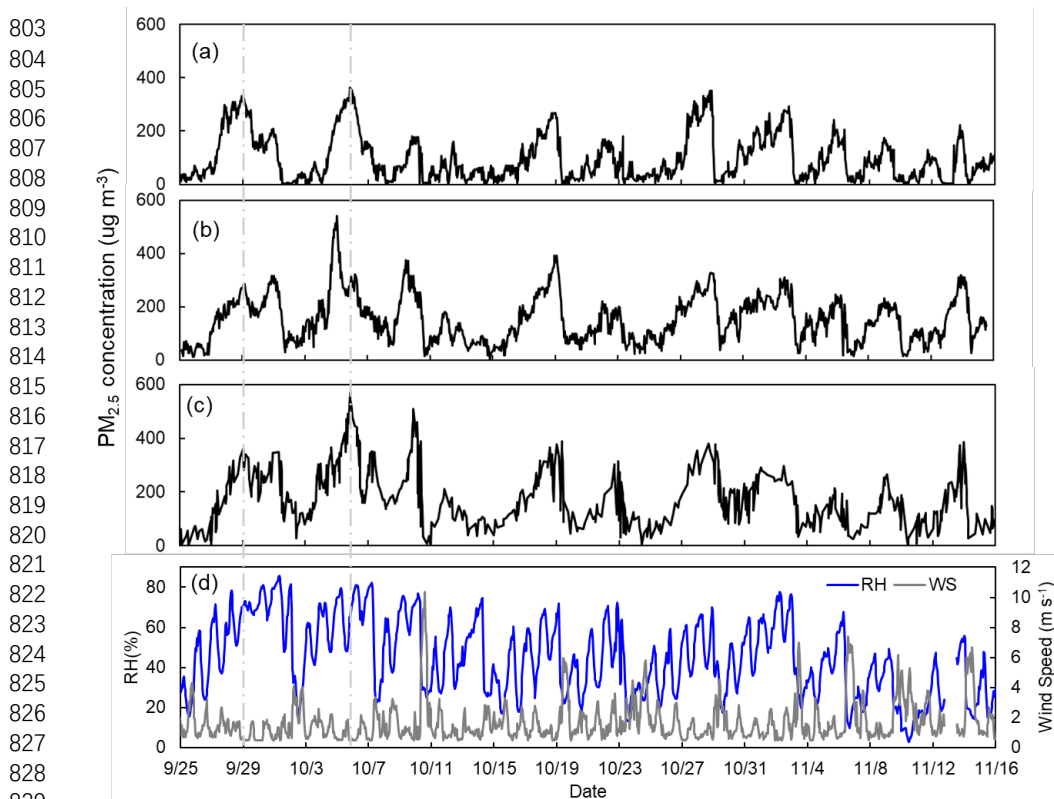748   Ramanathan, V.: Black carbon solar absorption suppresses turbulence in the atmospheric

749   boundary layer, Proc. Natl. Acad. Sci. USA, 113, 11794-11799,

750   10.1073/pnas.1525746113, 2016.

751 Wood, E. C., Canagaratna, M. R., Herndon, S. C., Onasch, T. B., Kolb, C. E., Worsnop, D.

752   R., Kroll, J. H., Knighton, W. B., Seila, R., Zavala, M., Molina, L. T., DeCarlo, P. F.,

753   Jimenez, J. L., Weinheimer, A. J., Knapp, D. J., Jobson, B. T., Stutz, J., Kuster, W. C.,

754   and Williams, E. J.: Investigation of the correlation between odd oxygen and secondary

755   organic aerosol in Mexico City and Houston, Atmos. Chem. Phys., 10, 8947-8968,

756   10.5194/acp-10-8947-2010, 2010.

757 Wu, G., Li, Z., Fu, C., Zhang, X., Zhang, R., Zhang, R., Zhou, T., Li, J., Li, J., Zhou, D., Wu,

758   L., Zhou, L., He, B. and Huang, R. Advances in studying interactions between aerosols

759   and monsoon in China, *Sci.* China: Earth Sci., 59, 1–16, 10.1007/s11430-015-5198-z,

760   2016.

761 Wu, G. Y., Brown, J., Zamora, M. L., Miller, A., Satterfield, M. C., Meininger, C. J.,

762   Steinhauser, C. B., Johnson, G. A., Burghardt, R. C., Bazer, F. W., Li, Y. X., Johnson, N.

763   M., Molina, M. J., and Zhang, R. Y.: Adverse organogenesis and predisposed long-term

764   metabolic syndrome from prenatal exposure to fine particulate matter, Proc. Natl. Acad.

765   Sci. USA, 116, 11590-11595, 10.1073/pnas.1902925116, 2019.

766 Wu, J. R., Bei, N. F., Hu, B., Liu, S. X., Wang, Y., Shen, Z. X., Li, X., Liu, L., Wang, R. N.,

767   Liu, Z. R., Cao, J. J., Tie, X. X., Molina, L. T., and Li, G. H.: Aerosol-photolysis

768   interaction reduces particulate matter during wintertime haze events, Proc. Natl. Acad.

769   Sci. USA, 117, 9755-9761, 10.1073/pnas.1916775117, 2020.

770 Xia, X., Chen, H., Goloub, P., Zhang, W., Chatenet, B., and Wang, P.: A compilation of

771   aerosol optical properties and calculation of direct radiative forcing over an urban region

772   in northern China, J. Geophys. Res.: Atmos., 112, 10.1029/2006JD008119, 2007.

773   Yuan, T., Li, Z., Zhang, R., and Fan, J. Increase of cloud droplet size with aerosol optical

774   depth: An observation and modeling study, J. Geophys. Res., 113, D04201,

775   doi:10.1029/2007JD008632, 2008.

776   Zhang, F., Wang, Y., Peng, J. F., Chen, L., Sun, Y. L., Duan, L., Ge, X. L., Li, Y. X., Zhao, J.

777   Y., Liu, C., Zhang, X. C., Zhang, G., Pan, Y. P., Wang, Y. S., Zhang, A. L., Ji, Y. M.,

778   Wang, G. H., Hu, M., Molina, M. J., and Zhang, R. Y.: An unexpected catalyst dominates

779   formation and radiative forcing of regional haze, Proc. Natl. Acad. Sci. USA, 117, 3960-

780   3966, doi/10.1073/pnas.1919343117, 2020.

781   Zhang, R., Li, G. H., Fan, J. W., Wu, D. L., and Molina, M. J.: Intensification of Pacific

782   storm track linked to Asian pollution, Proc. Natl. Acad. Sci. USA, 104, 5295-5299,

783   10.1073/pnas.0700618104, 2007.

784   Zhang, R., Khalizov, A. F., Pagels, J., Zhang, D., Xue, H., and McMurry, P. H.: Variability in

785   morphology, hygroscopicity, and optical properties of soot aerosols during atmospheric

786   processing, Proc. Natl. Acad. Sci. USA, 105, 10291-10296, 10.1073/pnas.0804860105,

787   2008.

788   Zhang, R., Wang, G., Guo, S., Zamora, M. L., Ying, Q., Lin, Y., Wang, W., Hu, M., and

789   Wang, Y.: Formation of Urban Fine Particulate Matter, Chem. Rev., 115, 3803-3855,

790   10.1021/acs.chemrev.5b00067, 2015a.

791   Zhang, R., Guo, S., Levy Zamora, M., and Hu, M.: Reply to Li et al.: Insufficient evidence

792   for the contribution of regional transport to severe haze formation in Beijing, Proc. Natl.

793   Acad. Sci. USA, 112, E2741, 10.1073/pnas.1503855112, 2015b.

794   Zhang, R., N.M. Johnson, Y. Li: Establishing the exposure-outcome relation between

795   airborne particulate matter and children's health, Thorax 76, doi.org/10.1136/thoraxjnl-

796   2021- 217017, 2021.

797   Zhang, X., Zhang, Q., Hong, C., Zheng, Y., Geng, G., Tong, D., Zhang, Y., and Zhang, X.:

798   Enhancement of PM2.5 concentrations by aerosol-meteorology interactions over China, J.

799   Geophys. Res.: Atmos., 1179-1194, 10.1002/2017JD027524, 2018.

800   Zhao, J., Zhang, R., Misawa, K. and Shibuya, K. Experimental product study of the OH-

801   initiated oxidation of m-xylene. J. Photoch. Photobio. A, 176, 199-207, 2005.

802

Atmospheric
Chemistry
and Physics
Discussions

Open Access
EGU

803
804
805
806
807
808
809
810
811
812
813
814
815
816
817
818
819
820
821
822
823
824
825
826
827
828
829

Figure 1. Time series of PM$_{2.5}$ mass concentration measured at three megacities over North China Plain (NCP), including (a) Beijing, (b) Baoding, and (c) Shijiazhuang from 25 September to 16 November, 2013, and (d) the associated relative humidity (RH, blue line) and 10-m wind speed (grey line) in Beijing. The PM$_{2.5}$ mass concentration and meteorological fields in Beijing are taken from Guo et al. (2014), and the PM$_{2.5}$ data for Baoding and Shijiazhuang are taken from https://air.cnemc.cn:18007/. Two severe haze episodes from 25-29 September and from 2-7 October are selected as the case studies in this work, and the two vertical dash lines label the time for the peak PM$_{2.5}$ concentration in Beijing.
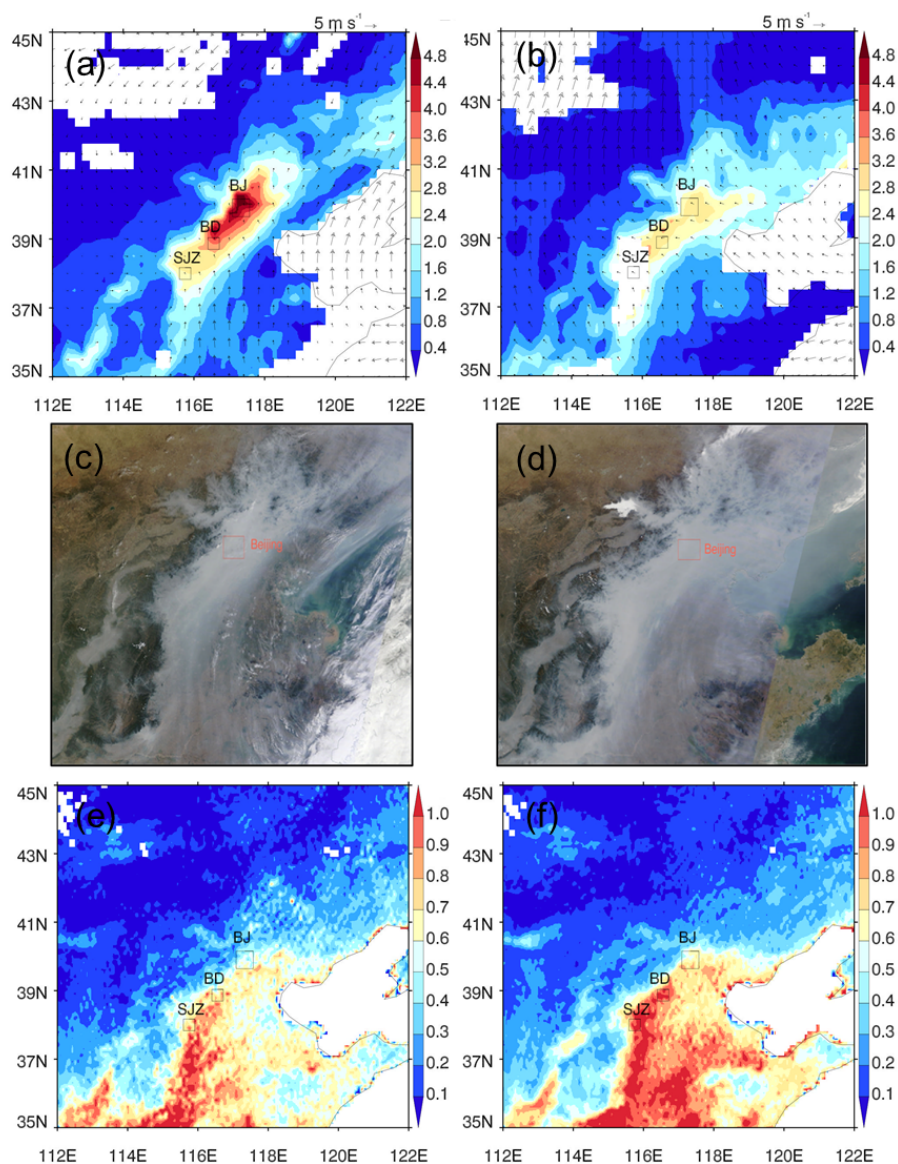
Figure 2. MODIS AOD (a-b) and visible images (c-d) illustrating the two severe haze episodes in Fig. 1. (a) and (c) correspond to 28 September, 2013, and (b) and (d) correspond to 5 October, 2013. (e) and (f) represent MODIS AOD of fall seasonal and annual mean in 2013. The megacities of Beijing (BJ), Baoding (BD) and Shijiazhuang (SJZ) are marked as squares. Wind field imposed on (a) and (b) is based on ECMWF reanalysis data.

Atmospheric
Chemistry
and Physics
Discussions
Open Access
EGU
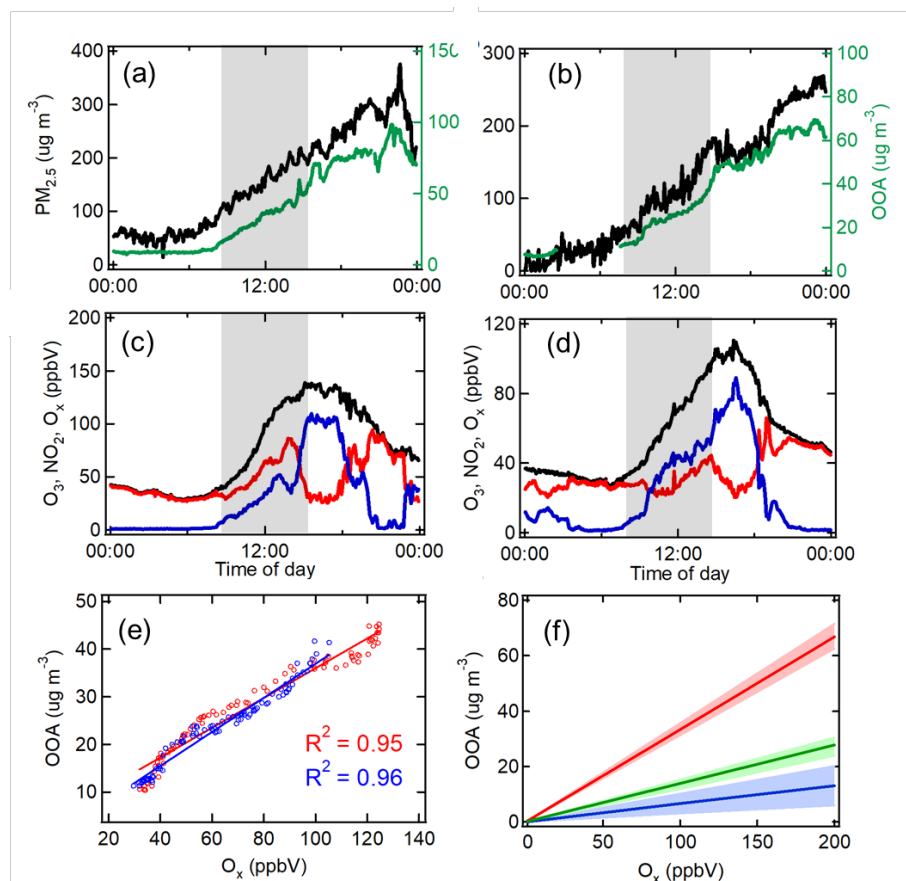
Figure 3. The temporal evolutions of measured PM$_{2.5}$ (black) and OOA (green) mass concentrations (a-b) and O$_3$ (blue), NO$_2$ (red), and O$_x$ (black) mixing ratios (c-d) during the early stages of the two haze episodes. (a) and (c) are for the episode starting on 27 September, 2013, and (b) and (d) are for the episode starting on 4 October, 2013. (e) represents linear regression between O$_x$ and OOA on 27 September (red circles) and 4 October (blue circles), 2013, using measurements at the transition periods (grey shadings (a-d)). (f) corresponds to the ratios of [OOA] changes to [O$_x$] changes (Δ[OOA]/Δ[O$_x$]) for Beijing (red), Mexico City (green) and Houston (blue). The ratios for Beijing are derived from this study, and the ratios for Mexico City and Houston taken from Wood et al. (2010). Color shadings in (f) represent the range between the minimum and maximum ratios.
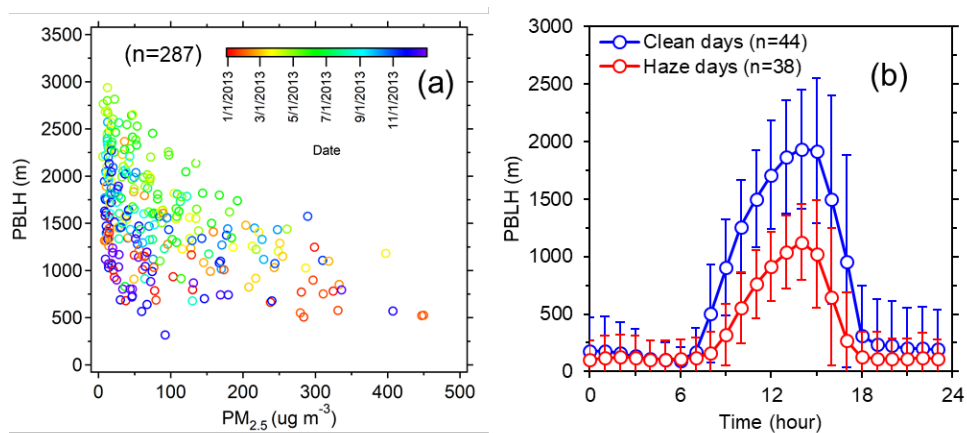
Figure 4. (a) Scattering plot for daily mean PBL height versus $PM_{2.5}$ concentration and (b) mean diurnal variations of PBL height averaged over clean days (daily mean $PM_{2.5}$ < 30 μg m^{-3}) and extremely hazy days (daily mean $PM_{2.5}$ > 200 μg m^{-3}) in 2013 at Beijing, China. n denotes the number of days used for plotting. The vertical lines in (b) denote ± 1 standard deviation. All the precipitation days were filtered out.

864
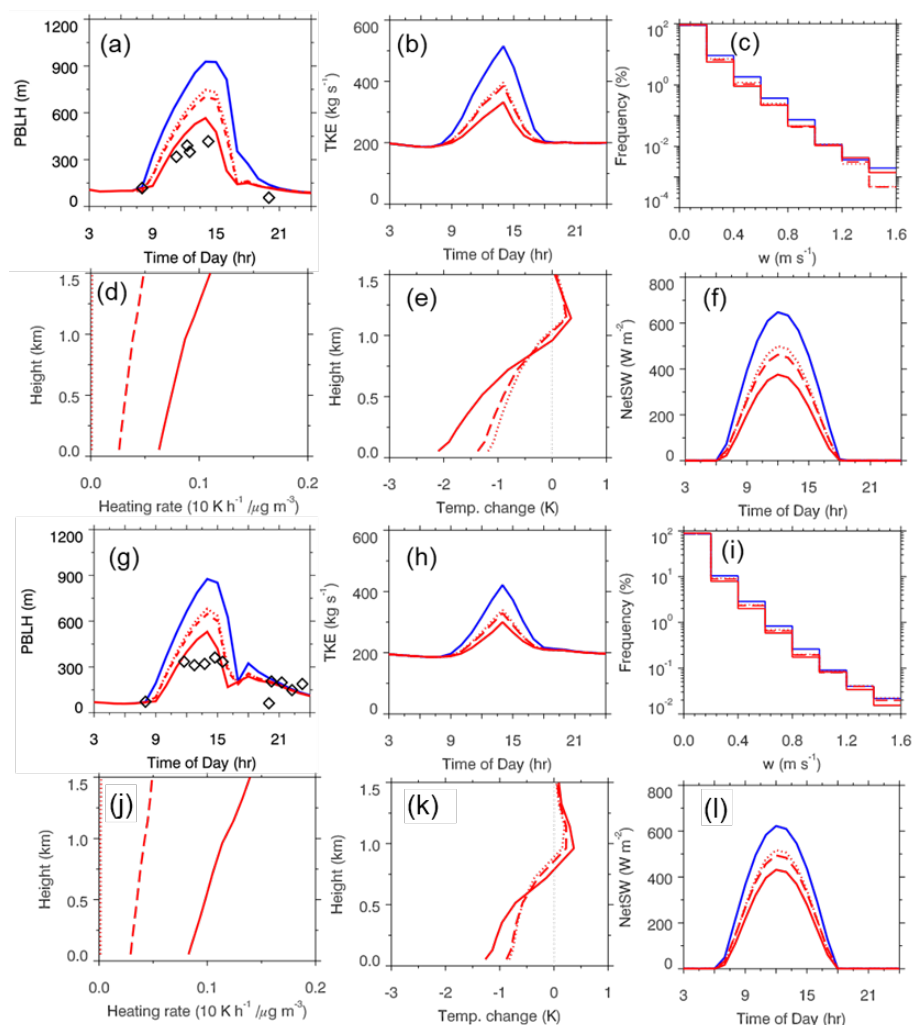
Figure 5. Simulated meteorological conditions and thermodynamic and dynamic feedbacks
under the clean conditions (blue solid) and the polluted conditions for the non-BC (red dot),
fresh-BC (red dashed), and aged-BC (red solid) cases. (a) and (g) correspond to simulated
diurnal variations of PBL height, (b) and (h) correspond to the diurnal variations of vertically
integrated TKE, (c) and (i) represent the frequency distribution of updraft. (d) and (j) are the
vertical profile of the shortwave heating rate per unit aerosol mass for the non-BC (red dot
line), fresh-BC (red dash line), and aged-BC (red solid line) cases. (e) and (k) are similar as
(d) and (j) but for the temperature changes. (f) and (l) are diurnal evolutions of net surface
shortwave radiation (NetSW). (a-f) are for EP1 and (g-n) are for EP2. The black hollow
squares in (a) and (g) denote measurements of PBL height from ceilometer.

875
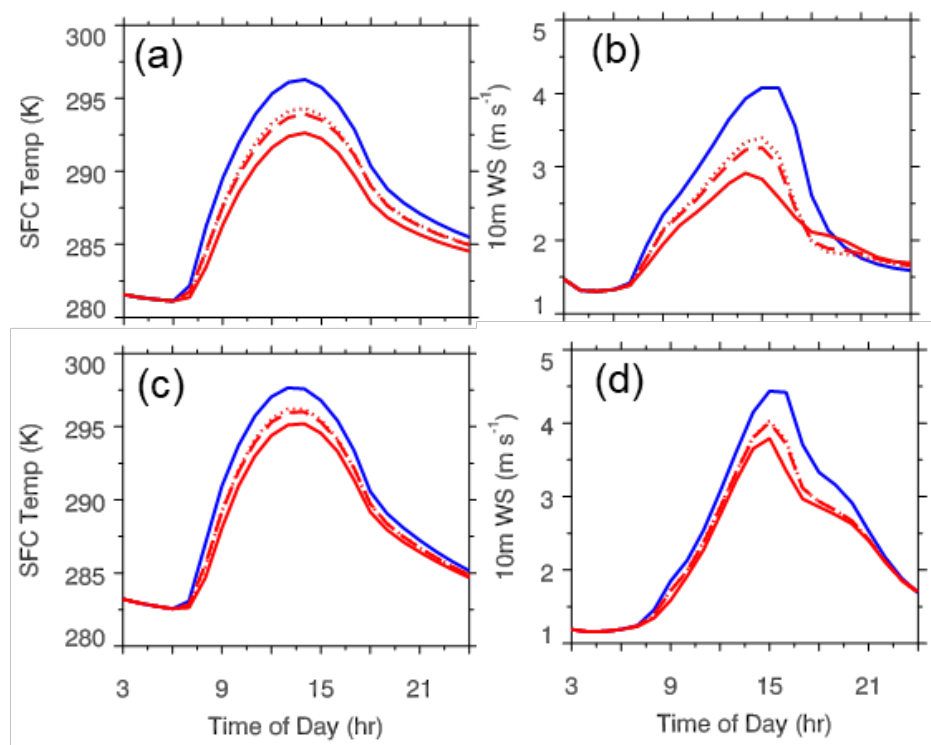
Figure 6. Temporal evolutions of surface temperatures (a and c) and 10-meter wind speeds (b and d) under the clean conditions (blue solid) and the polluted conditions for the non-BC (red dot), fresh-BC (red dashed), and aged-BC (red solid) cases. (a) and (b) correspond to EP1, and (c) and (d) correspond to EP2.
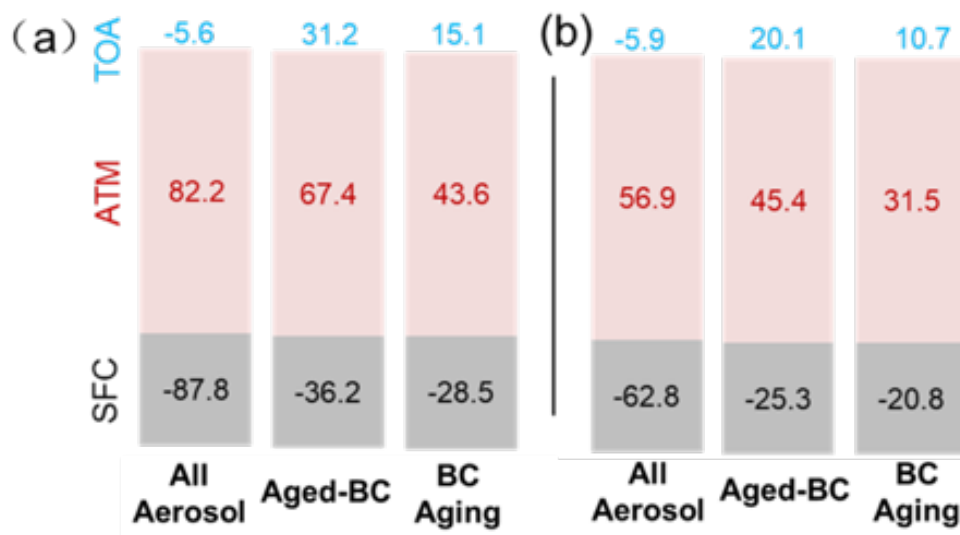
Figure 7. Aerosol direct radiative forcing for total aerosol (left column), aged-BC (middle column), and BC aging (right column) on the top of the atmosphere (TOA), in the atmosphere (ATM), and at the surface (SFC) for two severe haze days in Beijing. (a) and (b) correspond to EP1 and EP2, respectively. The forcing caused by BC aging corresponds to the difference in the simulations between the fresh-BC and aged-BC cases. The number denotes radiative forcing in the unit of W m^{-2}.